Modeling the Electrochemical Hydrogen Oxidation and Evolution Reactions on the Basis of Density Functional Theory Calculations

Egill Skúlason,[†,‡] Vladimir Tripkovic,[†] Mårten E. Björketun,[†] Sigrídur Gudmundsdóttir,[‡] Gustav Karlberg,[†] Jan Rossmeisl,[†] Thomas Bligaard,[†] Hannes Jónsson,[§,∥] and Jens K. Nørskov*[,†,∥,⊥]

Center for Atomic-scale Materials Design, Department of Physics, Building 311, Technical University of Denmark, DK-2800 Lyngby, Denmark, Science Institute, VR-III, University of Iceland, IS-107 Reykjavik, Iceland, Faculty of Science, VR-III, University of Iceland, IS-107 Reykjavik, Iceland, Center for Interface Science and Catalysis, SLAC National Accelerator Laboratory, 2575 Sand Hill Road, Menlo Park, California 94025, and Department of Chemical Engineering, Stanford University, Stanford, California 94305

Received: May 27, 2010; Revised Manuscript Received: August 20, 2010

Density functional theory calculations have been performed for the three elementary steps—Tafel, Heyrovsky, and Volmer—involved in the hydrogen oxidation reaction (HOR) and its reverse, the hydrogen evolution reaction (HER). For the Pt(111) surface a detailed model consisting of a negatively charged Pt(111) slab and solvated protons in up to three water bilayers is considered and reaction energies and activation barriers are determined by using a newly developed computational scheme where the potential can be kept constant during a charge transfer reaction. We determine the rate limiting reaction on Pt(111) to be Tafel−Volmer for HOR and Volmer−Tafel for HER. Calculated rates agree well with experimental data. Both the H adsorption energy and the energy barrier for the Tafel reaction are then calculated for a range of metal electrodes, including Au, Ag, Cu, Pt, Pd, Ni, Ir, Rh, Co, Ru, Re, W, Mo, and Nb, different facets, and step of surfaces. We compare the results for different facets of the Pt electrode to experimental data. Our results suggest that the most important parameter for describing the HOR or the HER activity of an electrode is its binding free energy of H. We present a detailed kinetic model based entirely on the DFT reactions and show that the exchange current follows a volcano curve when plotted against the H adsorption free energy in excellent agreement with experimental data.

1. Introduction

Any hydrogen-based energy conversion scenario relies on effective and cheap catalysts for oxidation and reduction of hydrogen.[1] Platinum-based catalysts are effective and stable for both hydrogen oxidation reaction (HOR) and hydrogen evolution reaction (HER) under acidic conditions as it is found in a polymer electrolyte fuel cell or electrolyzer. However, since Pt is rare and expensive there is a need for the development of electrodes made of cheaper materials. To be able to design new electrodes for the hydrogen evolution or oxidation reactions, it may well prove essential to acquire insight into their mechanism at the atomic level.[2−7]

It is generally accepted that the overall HOR/HER reaction $H_2 \leftrightarrow 2(H^+ + e^-)$, taking place at an electrode in contact with an electrolyte, involves three elementary reactions. In the first step, H_2 is dissociated and H adsorbed. This is accomplished either by the Tafel reaction $H_2 \rightarrow 2H^*$ (H* denotes hydrogen adsorbed on the surface) or by the Heyrovsky reaction $H_2 \rightarrow H^* + H^+ + e^-$. The adsorbed H is then discharged, following the Volmer route $H^* \rightarrow H^+ + e^-$. Despite intensive research efforts it is still unclear which of the two pathways, Tafel−Volmer or Heyrovsky−Volmer, dominates under different conditions even on the most studied electrode material, Pt. The Volmer reaction is usually considered fast[3] but the literature contains conflicting reports about the other two reactions. From some experimental studies it has been inferred that the Tafel reaction is the predominant mechanism and rate-limiting step on Pt(110)[2] and different facets of Pt.[4−6] This was recently supported by first principles calculations at the Pt(110)/water interface.[8] At the same time, other investigations report the Heyrovsky reaction to be the rate-determining step—both on Pt(100)[2] and on polycrystalline Pt.[7] In simulations a similar conclusion has been obtained for a single Pt atom[9] and on a diamond electrode.[10] The picture is equally confusing on the Pt(111) electrode surface.[2,11] The current view appears to be that different metal facets open up different reaction mechanisms for HOR and HER. Other studies, based on modeling the kinetics of HOR on Pt electrodes over the entire relevant potential region, conclude that the Volmer−Tafel pathway is dominating at low overpotentials whereas the Volmer−Heyrovsky route becomes important at high overpotentials.[12]

Most experimental insight about the mechanism has been inferred from rate measurements. Such a procedure will typically not provide conclusive evidence for a mechanism, since the measured rate depends on several elementary steps. Quantum chemical calculations can serve as a valuable complement. The calculations can be used to model electrochemical systems and have the potential to provide unique molecular-level information about processes at the interface. However, due to the complex environment it has only recently been possible to model electrochemical systems with first-principles methods.[8−11,13−22]

* To whom correspondence should be addressed. E-mail: norskov@stanford.edu.
[†] Technical University of Denmark.
[‡] Science Institute, University of Iceland.
[§] Faculty of Science, University of Iceland.
[∥] SLAC National Accelerator Laboratory.
[⊥] Stanford University.

10.1021/jp1048887
Published on Web 10/05/2010

Recently we introduced a general density functional theory (DFT) based model of the electrochemical half-cell that captures many of the features of the electrical double layer.[11] The atomic setup consists of a metal slab, hydrogen atoms (or other atomic species if required) adsorbed on the metal surface, and an electrolyte represented by water layers outside the surface. The electrical double layer is formed by adding extra hydrogen atoms to the water layer. The hydrogen atom spontaneously separates into a proton becoming solvated in the water and an electron ending up at the surface of the metal slab. We can vary the surface charge, and hence the potential, by changing the concentration of protons (hydronium ions) in the electrolyte. This is completely analogous to the experimental situation where the electrochemical double layer is set up by an equal number of electrons and counterions. It avoids the introduction of artificial counter-charge smeared out all over space[18] or located far from the surface.[19] The down side of our approach is that we need to treat large surface unit cells in order to vary the charge or potential semicontinuously.

A further challenge arises when studying chemical reactions involving charge transfer, as is the case for the Heyrovsky and Volmer reactions. In a real system, where the area of the interface can be considered infinite on an atomic scale, the electrode potential will stay fixed during single charge transfer reactions. However, since the simulation unit cells used in the calculations are relatively small, the charge, and hence the potential, will vary considerably along the reaction path. Sometimes this introduces large errors in the calculated reaction energies and activation barriers. To avoid this artifact, we recently devised a scheme that enables calculation of activation and reaction energies in the limit where the bias is constant during the reaction.[21] Since this scheme has been employed throughout this work a short review of the main ideas behind it will be given below.

In the present work, we study the HOR and HER in detail by means of first-principles DFT. Since the Pt(111) electrode is the most studied electrode for HOR and HER we first apply our detailed solid−liquid interface model to study the elementary steps over Pt(111). We conclude the Tafel reaction to be the rate-limiting reaction step, and a detailed analysis of the kinetics is carried out for that reaction. We study the structure-dependence of the reaction by comparing the calculated rate over Pt(111) to those of Pt(100) and Pt(110). We then determine the H adsorption energy at varying H coverage on various electrode materials, including different transition metals and various surface structures. Finally, we use the energy profiles as input to a kinetic model of the HOR/HER current. This enables direct comparison with experimental data.

2. Method

2.1. Calculation Details. The electronic structure calculations have been carried out with self-consistent DFT in a plane-wave pseudopotential implementation, with 26 Ry (354 eV) cutoff for both the plane waves and the densities.[23−25] Most calculations were performed with the DACAPO code, using the RPBE exchange-correlation functional.[26,27] However, the Pt(100) and the Pt(110) surfaces were treated by using the VASP code[28,29] and the revPBE functional. A few test calculations were performed to compare the two xc-functionals and the reaction energy differences were less than 0.07 eV in all cases. All activation barriers have been calculated with the nudged elastic band (NEB) method.[30,31]

To model the proton/electron transfer reactions—Volmer and Heyrovsky reactions—we have used the double layer model described in more detail below in Section 2.2. To keep the potential constant during charge transfer we apply an extrapolation scheme,[21] which is also explained in some detail later in this section. Since these barrier calculations are quite time-consuming, we have only performed the full extrapolation scheme on Pt(111) for the Volmer and Heyrovsky reactions. We have also performed such calculations of both the reactions over Ru(0001), Pd(111), and Au(111) for a few different potentials and in general they agree well with the Pt calculations. In all these barrier calculations the slabs have been modeled with 3 metal layers, but the surface dimensions have been varied: (3 × 2), (3 × 4), (6 × 2), (6 × 3), (6 × 4), and (6 × 8) repeated unit cells have been employed, with (4 × 6), (4 × 3), (2 × 6), (2 × 4), (2 × 3), and (2 × 1) *k*-point sampling, respectively. The two bottom layers of the slabs were fixed at the respective RPBE lattice constants, while the remaining atoms were allowed to adjust until the magnitude of all residual forces was less than 0.01 eV/Å.

For the Tafel reaction and H adsorption it has been shown that the reaction energies and activation energies are almost unaffected by water, electric potentials, and electric fields.[11,32] This is not surprising since there is no electron transfer to and from the electrode during this reaction ($2H^* \rightarrow H_2$) and the dipole of the adsorbed H is small in the direction perpendicular to the surface. Hence these effects can be neglected and only a surface slab and adsorbed hydrogen have to be included in the atomic model. This makes the problem computationally much less demanding. We can thus afford calculating the Tafel reaction and H adsorption energies as a function of H coverage for a large set of close-packed FCC, HCP, and BCC surfaces and also for other facets and steps. In these calculations the close-packed surfaces are modeled with three layers where the two bottom layers are kept fixed while the top layer is allowed to relax with the adsorbed hydrogen atoms. Pt(100) is modeled by using four layers, where the two bottom layers are fixed while the two top layers are relaxed with the hydrogen atoms. A test calculation is carried out for the Pt(100) surface having three layers instead of four layers, where the two bottom layers are fixed and the top layer is relaxed with the hydrogen atom. H binds slightly stronger to four Pt layers than to three Pt layers, or by less than 0.04 eV. The close-packed surfaces are typically modeled with (2 × 2) unit cells and (4 × 4) *k*-points but in a few cases we have increased the unit cells to (3 × 2), (4 × 4), and (6 × 4) in order to represent coverages close to an important discontinuity in the adsorption energy, appearing at 1 ML H coverage. This point will be clarified later in Sections 2.4 and 3.4.1. The (211) steps have three close-packed layers underneath the step and a (2 × 3) unit cell with (4 × 4) *k*-point sampling. The Pt(110) surface is modeled with 8 Pt layers in total with a (3 × 4) unit cell and (4 × 4) *k*-point sampling.

2.2. Model of the Electrochemical Double Layer. A typical setup of the calculation is illustrated in Figure 1. When adding an additional H atom into the first water layer, the electron from this H atom spontaneously enters the metal slab and a solvated hydronium ion (H_3O^+) is formed. In Figure 1 the charge iso-surfaces are plotted when having a solvated proton in the first water bilayer out of three water bilayers in total. The iso-surfaces are constructed by calculating the charge density differences of the whole system ($\rho_{Pt+e^-+water+H^+}(\mathbf{r})$) and two uncharged reference systems, when having the Pt slab and neutral water above it in one supercell ($\rho_{Pt+water}(\mathbf{r})$) and the additional H atom in another cell ($\rho_H(\mathbf{r})$):

$$\rho_{\text{difference}}(\mathbf{r}) = \rho_{\text{Pt+e}^-\text{+water+H}^+}(\mathbf{r}) - \rho_{\text{Pt+water}}(\mathbf{r}) - \rho_{\text{H}}(\mathbf{r}) \quad (1)$$

Figure 1 shows that the positive charge is localized in the first water bilayer and does not spread out to the water above. In other words, the positive charge is solvated in a two-dimensional plane at the solid−liquid interface. This indicates that we can solvate the proton by only using one water bilayer above the slab.

In Figure 2 the charge iso-surfaces are plotted at several proton concentrations/electrode potentials. Here, we use a single water bilayer above a Pt(111) slab. The positive (blue) charge is quite localized around the H_3O^+ complex but some positive charge is associated with the three water molecules in the solvation cell. The solvation shell is in-between the Zundel structure[33,34] where the proton is shared between two water molecules forming an $H_5O_2^+$ complex, and the Eigen structure[35,36] where the hydronium ion is hydrogen bonded to three water molecules, forming an $H_9O_4^+$ complex. Here the solvation structure is two-dimensional in the vicinity of the surface, whereas the solvation shells are three-dimensional in bulk water.[37]

We note that the negative charge (purple) of the additional electrons on the surface is rather localized underneath the proton involving of the order 6−9 Pt atoms. This suggests that models that describe the double-layer as homogeneous along the surface may not include all relevant electrostatic effects in the calculation. There are, however, a number of situations where such effects are of minor importance.

Each proton concentration corresponds to a certain electrode potential (U) versus the normal hydrogen electrode (NHE). The U values are varying here from negative to positive values. The link to an absolute U scale will be discussed in the following.

In ref 21 we introduced a direct link between the thermodynamic definition of the NHE electrode and the calculated work function (WF). Hence, we have an internal definition of the absolute potential scale for the solid/liquid interface as it is charged with protons and electrons. The total free energy or the integral free energy, G_{int}, is calculated per surface metal atom (or surface area) relative to H_2 in the gas phase:

$$G_{\text{int}} = (G(N,n) - G(N,0) - n\mu_{\text{H2}}/2)/N \quad (2)$$

where N is the number of surface metal atoms in the surface unit cell and n is the number of protons in the double layer (per super cell). In Figure 3 we have calculated the integral free energy of the charged double layer including 1, 2, and 3 water bilayers, see the atomistic structures in systems a, b, and c of Figure 3, respectively. The variation in the WF (U scale) comes from variations of the proton/electron concentration. The reference WF values we need to shift the parabolic functions in order to have the minimum in free energy at $U = 0$ V vs NHE are very similar for the different water layer systems: 5.28 V for 1 and 3 water layers and 5.13 for the 2 water layers. The experimental value of the WF of the NHE compared to vacuum is usually measured to be 4.44 ± 0.02 V[38] while a value of 4.85 V has also been reported.[39]

It should be noted that when considering more than one water bilayer we have altered the orientations of the water molecules in the second and third layers in order to avoid building up net dipoles from the water network. The first water bilayer has an H-down structure in systems a−c in Figure 3 where structures b and c have no net dipoles in the remaining layers. System d has an H-up structure of the first water bilayer but that system will be discussed at a later point in this section. Since we are using an atomistic model of the water at the interface, the reference value in our internal measure cannot be compared directly with the experimental value, obtained at real conditions and at room temperature. In reality the water structure will be thermally distorted and not having every other water molecule of the first water layer pointing the O−H bond toward the surface as structures a−c in Figure 3.

Schnur and Groβ have recently studied the metal−water interface with ab initio molecular dynamic simulations at room temperature.[40] There it is shown explicitly that the first water layer is neither purely a H-down structure nor a H-up structure, but a mixture of them both. The WF of the thermalized metal−water interface is also found to be somewhere in between the WF of the H-down and the H-up structures.

We calculate the WF of a Pt(111) slab having one water layer to be 6.7 V for the water-down structure while it is 4.1 V with the water-up structure. This 2.6 V difference between the two water structures on Pt(111) is to be compared with a value of around 2.2 V difference for the same systems in the calculations by Schnur and Groβ.[40] Similar differences in WF are found for these two water layer models for all other metals considered in that study.

The WF's time evolution is reported only for the Ru(0001)−water system.[40] At time zero, the difference in WF between H-up and H-down is around 2.5 V. After 6 ps simulation time the WF of these two systems have reached the same value, which is around 30% from the H-down WF value and 70% from the H-up value. That means that at room temperature, the neutral water layer and its WF is somewhere in between the H-down and the H-up structure, where presumably more water dipoles are pointing toward the surface than from it. It should be noted that there is only a single water layer included in the study by Schnur and Groβ and these results could change when more water layers are included.

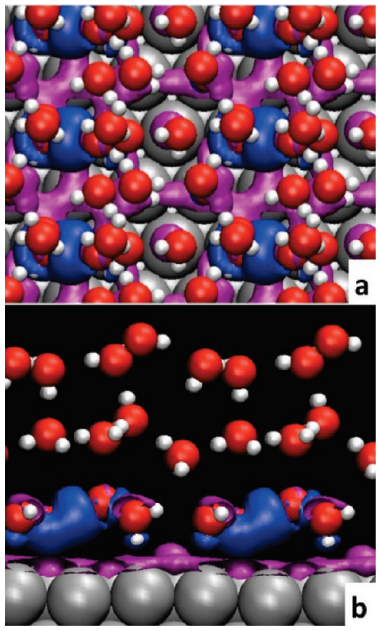

Figure 1. (a) Top view and (b) side view of a solvated proton in 3 water layers ontop of a Pt(111) electrode. The blue iso-surfaces (iso-value: −0.0018 e bohr^{-3}) are regions of positive charge around the proton solvated in the water. The purple iso-surfaces (iso-value: +0.0012 e bohr^{-3}) on the Pt surface are regions of negative charge at the electrode surface. In this case the proton concentration is very high (1 proton per 6 surface atoms).

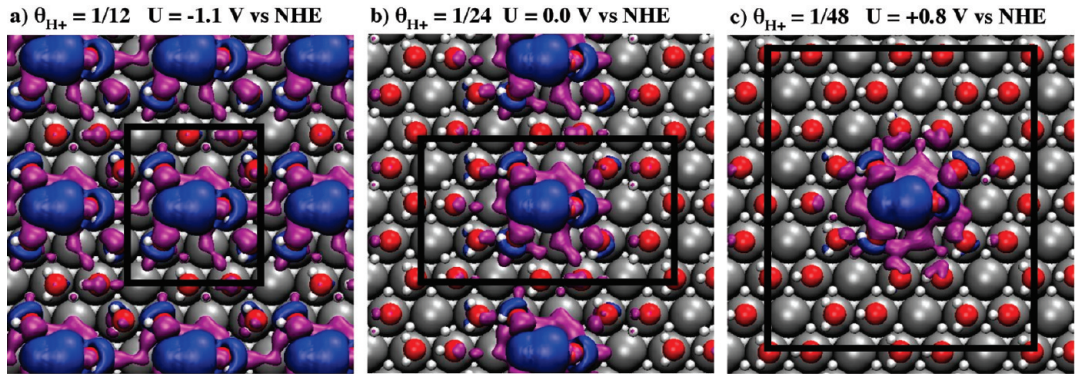

Figure 2. Solvated protons in a water bilayer ontop of the Pt(111) slab. The blue iso-surfaces are positive charge of the proton and the purple iso-surfaces are negative charge on the surface. The figures show different proton concentrations θ_{H^+} in the unit cells, i.e. the unit cells are enlarged but in each case there is 1 proton per unit cell: (a) 1 proton per 12 Pt surface atoms, (b) 1 proton per 24 surface atoms, and (c) 1 proton per 48 surface atoms. The iso-values are -0.0005 e bohr^{-3} in all cases for the positive charge. For the negative charge the iso-values are $+0.0008$, $+0.0005$, and $+0.0003$ e bohr^{-3} for the 1/12, 1/24, and 1/48 proton concentrations, respectively.

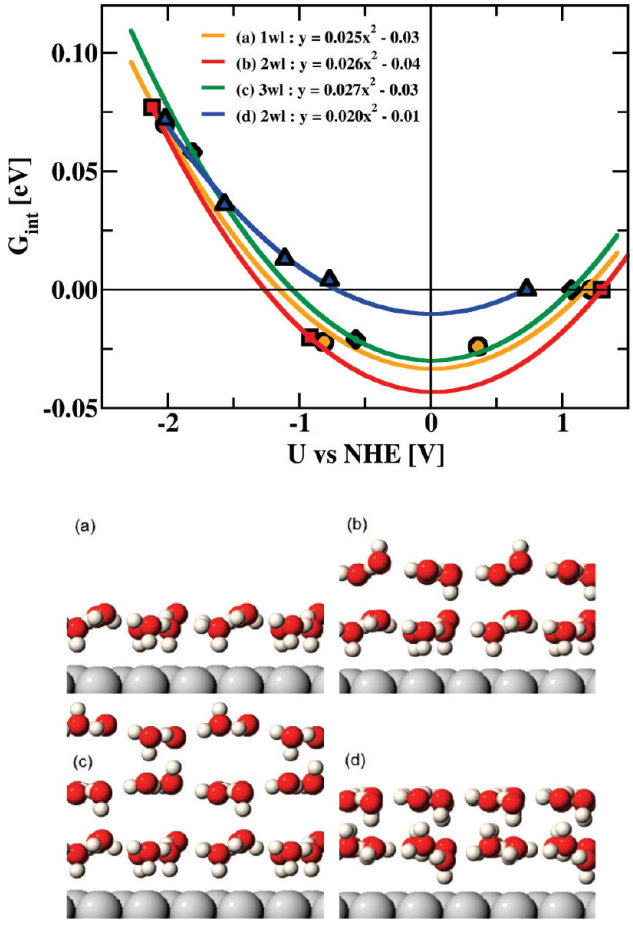

Figure 3. The integral free energy stored in the double layer as a function of the electrode potential when having (a) 1, (b) 2, and (c) 3 water layers with a H-down configuration of the first water bilayer and (d) 2 water layers with a H-up configuration of the first water bilayer on a Pt(111) electrode. The H coverage at the surface is 1 ML in parts a−c, whereas it is 0 ML in part d.

If we would use the water-up structure throughout this investigation, our internal measure of the reference WF would be approximately 2.7 V instead of approximately 5.3 V for the water-down structures. In reality we might have some waters pointing up and others pointing down, as suggested by Schnur and Groβ.[40] By assuming the same 30%/70% difference from the H-down/H-up WFs on the Pt(111) surface as found on the Ru(0001) surface due to thermalization[40] the reference WF value would be 4.5 V, in close agreement with the experimental value of 4.44 V.

There seems to exist many different water structures which all are very close in energy.[41] Since all energies of interest in the following are energy differences, they are not sensitive to the exact model of the water as long as we are consistently using the same model in calculating the energy differences and as long as we choose a reasonable model in a local minimum structure. A strength of the approach is that we have an internal reference point defining the zero of the potential for the exact structure we are using.

More work is needed to address the question of water structures further but that may have to await exchange-correlation functionals that can confidently determine van der Waals interactions. In the meanwhile we note that the curvature of the parabolas can be used to determine the capacitance of the double layer in excellent agreement with experiment. We get $C = 22.7$ μF/cm^2 for 1 water layer, $C = 23.6$ μF/cm^2 for 2 water layers, and $C = 24.5$ μF/cm^2 for 3 water layers, while the experimentally measured value is $C = 20$ μF/cm^2 on Pt(111).[42] This good comparison to experiments and the small difference in modeling the system with 1, 2, or 3 water layers provides confidence in the present description and indicates that a single water bilayer is sufficient to describe the interface. We use this observation when analyzing the Volmer and the Heyrovsky reactions in the rest of the study.

In Figure 3 we have included the integral free energy of systems having H-up configuration of the first water bilayer whereas the second water bilayer has a H-down structure. The atomistic structure is shown in system d of Figure 3. This model system is unrealistic in the sense that the first bilayer has an H-up structure while at the same time the surface is negatively charged. It is an extreme case and will be included later on in next sections to show that the energy differences that we calculate throughout this study are not sensitive to our chose of water models.

2.3. Extrapolation Scheme. In the model presented above, where the ions are explicitly localized in the Helmholtz layer, a problem arises when these ions react with electrons from the surface. Since we have periodic boundary conditions and are limited to using finite size unit cells, performing one proton−electron transfer reaction in a unit cell corresponds to a simultaneous transfer in each unit cell. Since the ions set up the potential and the field, performing such a reaction changes the potential of the electrode along the reaction path. That can

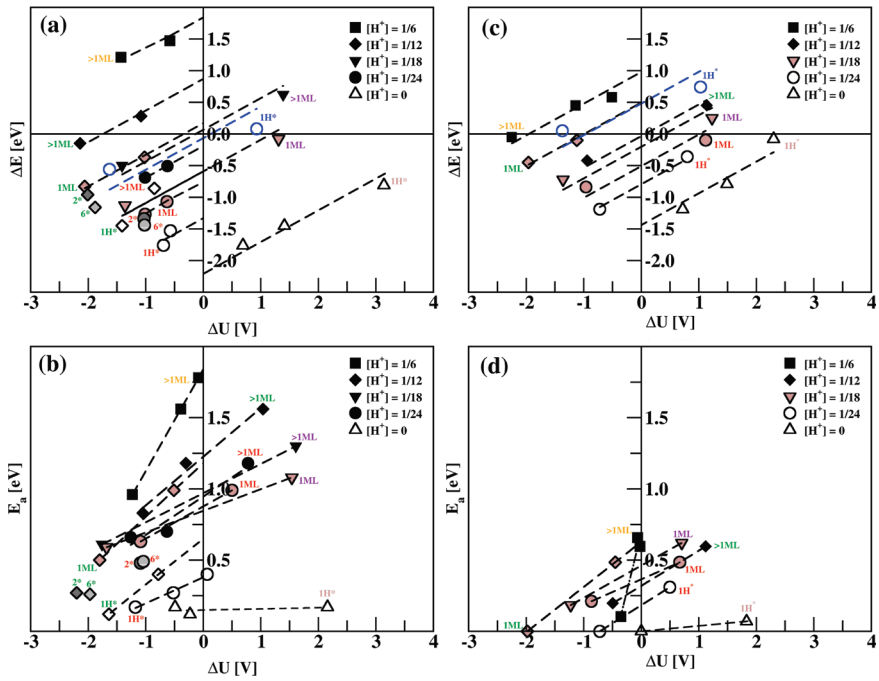

Figure 4. The reaction energy (a and c) and the activation energy (b and d) for the hydrogen oxidation reaction via the Heyrovsky reaction (a and b) and the Volmer reaction (c and d) on a Pt(111) electrode vs the change in electrode potential ΔU for those reactions. Each set of data points connected by a line corresponds to a fixed concentration of protons and hence a fixed potential. The crossing with $\Delta U = 0$ signifies the reaction energy or the activation energy for the Heyrovsky or the Volmer reaction when the bias does not change during the reaction. All the data points are calculated with model system shown in structure a of Figure 3, except for the blue circles where structure d of Figure 3 was used. $\chi^2 = 0.00-0.07$ for all lines except for the blue circles; $\chi^2 = 0.20$ in panel a and $\chi^2 = 0.13$ in panel c.

affect the energetics considerably. This problem is most severe for the smallest unit cells we consider here in which the bias can change by up to 3.5 V for the Heyrovsky reaction.

The approach we take to circumvent this problem is referred to as "the extrapolation scheme" and has been explained in detail elsewhere.[21] When calculating reaction energies and activation energies for a charge transfer reaction such as the Heyrovsky or the Volmer reactions, we calculate the energies for several different unit cell sizes. We extrapolate the results to the limit of an infinitely large unit cell or equivalently to the limit where the change in potential, ΔU, during the reaction approaches zero. That mimics the situation in a real electrochemical system. This is explained in detail below.

The Heyrovsky reaction for the HOR direction is shown as an example, but the approach can be used for any kind of charge transfer surface reaction. We extrapolate to $\Delta U = 0$, where ΔU is the difference of the initial state's (IS) and final state's (FS) work functions (WF). The variation in ΔU is obtained by using unit cells of different sizes, N, with a number of charges, n, determined so that the surface concentration of charge, $\theta = n/N$, is fixed.

In Figure 4a the calculated reaction energy, $\Delta E = E_{FS} - E_{IS}$, for HOR is plotted as a function of ΔU for different values of the surface charge density, θ, or equivalently potentials in the FS when $\Delta U < 0$ and IS when $\Delta U > 0$. The differences in energies are always presented for the same reaction direction, here for the HOR direction. The differences in WF are calculated with respect to the state we are extrapolating to. Take for example the data set for $\theta = 1/6$ (filled squares) where both of the FSs are the same, having 2 protons in a (6×2) cell and 4 protons in a (6×4) cell. The IS (having H_2 in the gas phase), however, do not have the same proton concentration, 1/12 and 3/24, respectively. In this case we calculate $\Delta U = WF_{FS} - WF_{IS}$, since both systems have the same FS proton concentration, 1/6. If we now extrapolate these data points to $\Delta U = 0$ we are in fact extrapolating to the FS proton concentration. This limit describes the situation where the IS and FS would have the same proton concentration.

If we now take exactly the opposite example, where we extrapolate to $\theta = 0$ (open triangles), all the IS have no protons in the water bilayer. The FS for the HOR direction all have 1 proton in (6×4), (3×4), and (3×2) unit cells. This difference in concentration results in the change in WFs. In this case, since we are extrapolating to $\theta = 0$ of the IS, ΔU is calculated as $WF_{IS} - WF_{FS}$.

As can be seen, we always subtract the WF of the states that are not having the same proton concentration from the WF of the states that have the same proton concentration. For the reaction energy versus ΔU this only results in a sign change of ΔU. We will, however, see that this formalism is important to use in the right way when doing extrapolations for the activation energies since the difference between the WF of the TS is not the same if we calculate it relative to the WF_{IS} or the WF_{FS}, since the WF_{TS} is not necessarily exactly in the middle between the WF of the IS and FS.

When plotting the reaction energy as a function of the difference in potential as explained above an approximately linear dependence is observed and we propose that by extrapolating the result to $\Delta U = 0$ we obtain a good approximation to the true value of the reaction energy in an infinite unit cell. The slope of this line should be 1/2, since we are transferring one charge in a capacitor.[21] This is exactly what we find in Figure 4a. The lines are fitted to the calculated data using a slope of 1/2.

The same approach can be used to estimate the activation energy of HOR via the Heyrovsky reaction, see Figure 4b. The calculations are again done in unit cells of varying surface area. The activation energy is obtained via the NEB method and is always calculated for the HOR direction in this example, $E_a = E_{TS} - E_{IS}$, where E is the total energy. The differences in

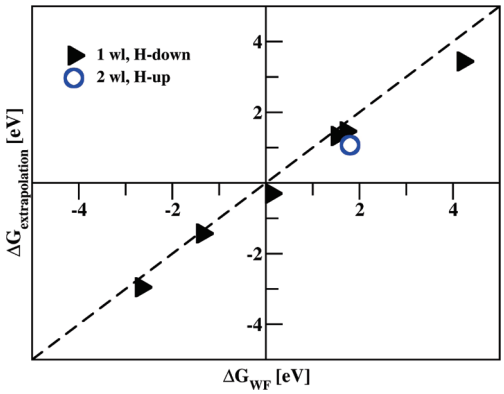

Figure 5. The free energy, $\Delta G_{\text{extrapolation}}$, of the two-electron process of the summed Heyrovsky and Volmer reaction from the combined extrapolations in Figure 4, parts a and c, as a function of the free energy, $\Delta G_{\text{WF}} = -2U$, when U is determined from the work function (WF) of the systems. Two different models of water bilayers are shown; 1 water layer with H-down configuration (black triangles) and 2 water layers with an H-up configuration of the first bilayer and an H-down configuration of the second bilayer (blue circle). The dashed line is $y = x$.

potentials, ΔU, are calculated in a similar way as for the reaction energy, where we take the WF of the state we are extrapolating to and we subtract the WF of the TS from that. In the case of $\theta = 1/6$ we subtract the WF of the TS from the WF of the FS; $\Delta U = \text{WF}_{\text{FS}} - \text{WF}_{\text{TS}}$, where the FS have $\theta = 1/6$.

As before, a similar procedure is used when extrapolating to $\theta = 0$ where all the IS have no protons in the water bilayer. ΔU is now $\text{WF}_{\text{IS}} - \text{WF}_{\text{TS}}$. In Figure 4b we have also in some cases interpolated from both negative and positive regions, where we have used a mixture of the two ΔU values explained above. In this case we always interpolate to the same proton concentration, where in some cases it is in the IS whereas in others it is in the FS. The data points are now both on the left side and the right side of $\Delta U = 0$, and we draw a straight line in between and read off the intercept at $\Delta U = 0$. For E_a we have not determined the slope of the ΔU dependence a priori.

The same approach can now be applied to the Volmer reaction. The extrapolated and the interpolated values (intercepts) are the reaction and activation energies when the bias does not change during the discharge reaction $\text{H}^* \rightarrow \text{H}^+ + \text{e}^-$. These are shown in Figure 4, parts c and d, respectively.

Let us now consider the HOR direction. Figure 4a contains the reaction energy of the Heyrovsky reaction, $\text{H}_2 \rightarrow \text{H}^+ + \text{e}^- + \text{H}^*$, while Figure 4c contains the reaction energy of the Volmer reaction, $\text{H}^+ + \text{e}^- + \text{H}^* \rightarrow 2\text{H}^+ + 2\text{e}^-$, both at several electrode potentials. If the Heyrovsky reaction is added to the Volmer reaction (at some fixed electrode potential) we obtain the overall HOR, $\text{H}_2 \rightarrow 2\text{H}^+ + 2\text{e}^-$, at several discrete electrode potentials. The reaction energy values are converted into reaction free energy values by including appropriate values for the ZPEs and vibrational entropy, which will be discussed in more detail in Section 2.4. The free energy of the overall HOR should be equal to two times the electrode potential, $\Delta G_{\text{HOR}} = -2U$, since two electrons are involved in this overall reaction. See ref 43 and section 2.4, eq 8, and section 3.1.4 below for more details. Notice that the effect of the H* adsorption energy of the individual reactions cancels out when the two reactions are added together. This is indeed what is observed in Figure 5 where the free energy $\Delta G_{\text{extrapolation}} = \Delta G_{\text{Heyrovsky}} + \Delta G_{\text{Volmer}}$ is plotted as a function of the free energy coming from the U deduced from the work function, $\Delta G_{\text{WF}} = -(U_{\text{Heyrovsky}} + U_{\text{Volmer}})$, for systems having the same proton concentrations and hence similar electrode potentials.

Figure 5 shows clearly that the energetics of the Heyrovsky and Volmer reactions are not dependent on the model of the water used. Here we use both a model system having only a single water bilayer with an H-down configuration (Figure 3a) and a more unrealistic two-water layer model with an H-up configuration in the first layer (Figure 3d). Overall, we have a one-to-one correspondence between free energies from the extrapolation scheme and free energies deduced from the WF, when we use a U scale that is insensitive of the water model.

2.4. Hydrogen Coverage-Dependent Electrode Potential Scale. As mentioned above, the energetics of adsorbed H is not affected by including water, electric fields and potentials in the calculations, and the same is true for the energetics along the reaction path for the Tafel reaction. To assign an electrode potential scale to that reaction it is therefore not necessary to use the detailed atomistic double layer model presented above. However, since the activation barrier of the Tafel reaction is affected by the H coverage on the surface, we introduced another type of U-scale for that reaction.[11] This will be reviewed again here in the following.

The integral H adsorption energy is defined by

$$E_{\text{int}}(\theta_{\text{H}^*}) = (E(\text{surface} + n\text{H}^*) - E(\text{surface}) - n/2E(\text{H}_2))/N \quad (3)$$

where $E(\text{surface} + n\text{H}^*)$ is the energy of the surface plus n hydrogen adsorbates, $E(\text{surface})$ is the energy of the clean surface, $E(\text{H}_2)$ is the energy of hydrogen molecules in the gas phase, N is the number of surface metal atoms in the super cell, and $\theta_{\text{H}^*} = n/N$ is the H coverage. E_{int} is the integral energy or the total adsorption energy of all the H atoms adsorbed on the surface (relative to H_2 in the gas phase) per surface metal atom.

To calculate the differential H adsorption energy as a function of the H coverage we multiply the $E_{\text{int}}(\theta_{\text{H}^*})$ in eq 3 with N and take the derivative with respect to n

$$\Delta E_{\text{H}^*} = E_{\text{diff}}(\theta_{\text{H}^*}) = \delta(N^*E_{\text{int}}(\theta_{\text{H}^*}))/\delta n = N^*\delta E_{\text{int}}(n/\text{N})/\delta n = N(E_{\text{int}}(n/\text{N}) - E_{\text{int}}((n-1)/N))/\Delta n \quad (4)$$

and $\Delta n \equiv 1$.

The differential adsorption free energy is calculated as:

$$\Delta G_{\text{H}^*} = \Delta E_{\text{H}^*} + \Delta(\text{ZPE}) - T\Delta S \quad (5)$$

where $\Delta(\text{ZPE})$ and ΔS are the differences in zero point energy and entropy, respectively, between the adsorbed hydrogen atoms and the hydrogen molecules in the gas phase. Greeley and Mavrikakis have calculated ZPE of adsorbed H on a range of transition metal surfaces using normal-mode analysis (NMA) with DFT calculations.[44] All ZPE are between 0.14 and 0.18 eV/H* for H adsorbed on FCC hollow sites. We calculate $TS_{\text{vib,H}^*} = 0.01$ eV/H* at 300 K on FCC hollow site on Pt(111) where the vibrational entropy is calculated by:[45]

$$S_{\text{vib}} = Nk_{\text{B}}\{\beta\varepsilon/(e^{\beta\varepsilon} - 1) - \ln(1 - e^{-\beta\varepsilon})\}$$

for N independent harmonic oscillators. Here, $\beta = 1/k_{\text{B}}T$ and ε is the total vibrational energy obtained with NMA DFT

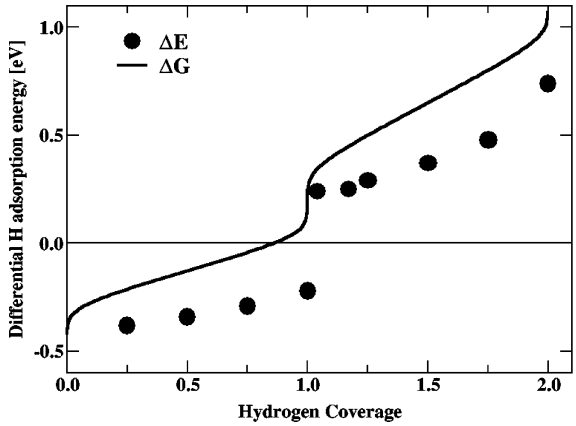

Figure 6. Differential H adsorption energy and free energy on Pt(111).

calculations. The ZPE of 0.27 eV/H_2 and TS of 0.41 eV/H_2 at 300 K of H_2 in the gas phase are taken from standard molecular tables.[46] Adding these values together, using eq 5, we get 0.22 eV/H* that we need to add to the electronic energy to get the free energy. Here we use a value of $ZPE_{H^*} = 0.16$ eV/H*, in between the $ZPE_{H^*} = 0.14-0.18$ eV/H* from Greeley and Mavrikakis.

We also need to include the configuration part of the entropy of the adsorbed H*.[11,32] The differential configurational entropy, $dS_{config}/d\theta_{H^*}$, is estimated by

$$dS_{config}/d\theta_{H^*} = k_B \ln((1-\theta_{H^*})/\theta_{H^*}) \quad (6)$$

(for $0 < \theta_H < 1$) which previously has been found to compare well with Monte Carlo simulations.[32]

Figure 6 shows the calculated differential H adsorption energies on Pt(111). It also contains the full free energy profile at 300 K. The difference between the full profile and the corresponding differential adsorption energy curve demonstrates the contribution to the differential free energy from the ZPE and the entropy. H adsorbs in 3-fold FCC sites up to a coverage of 1 ML. When exceeding 1 ML, additional H starts occupying on-top sites. At room temperature, ΔG_{H^*} is negative on Pt(111) as long as $\theta_{H^*} \leq 0.86$ ML in this model, which means that the surface will be nearly covered at $\Delta G_{H^*} = 0$.

The hydrogen coverage will be dependent on the potential via the reaction:

$$H^+ + e^- + * \rightarrow H^* \quad (7)$$

At standard conditions (298 K, pH 0, 1 bar H_2) and $U = 0$ V vs NHE, the left-hand side is in equilibrium with hydrogen gas. At finite bias, U, the chemical potential of the electron will be linearly dependent on the bias. The reaction free energy of eq 7 can be written as:[11,13]

$$\Delta G_{H^*}(U) = \Delta G_{H^*} - eU \quad (8)$$

$\Delta G_{H^*} = -eU$ defines the chemical potential of H*. If we make this conversion of scales in Figure 6, i.e. changing ΔG_{H^*} to $-eU$, we find that the coverage will be about 0.86 ML at $U = 0$ V vs NHE on Pt(111).

By calculating the free energy of H adsorption as a function of H coverage as in Figure 6 we can now convert the free energy scale to an electrode potential scale, or U scale $U = -\Delta G/e$. With this we have established a simple U scale, which is dependent on the H coverage. This is exactly what happens when measuring a cyclic voltammogram. When the bias is decreased from +0.4 V vs NHE the H starts to adsorb on the surface via the Volmer reaction. At $U = 0$ the surface is nearly covered with H and hydrogen gas is formed. The measured H coverage is 2/3 ML[3] when the evolution starts whereas we calculate 0.86 here. Recently, it has been concluded experimentally that the H coverage is higher than 2/3 ML at the reversible potential and a full monolayer is reached at −0.1 V vs NHE.[47]

We note that in the case of interacting adsorbed H atoms, the expression, eq 6, for the configurational entropy is not entirely correct. We have, however, also made Monte Carlo simulations and find the differences to be very small. We will return to this point later in section 3.2.

3. Results

In this section we will start by discussing the results obtained for Pt(111) where we calculated all the elementary steps for HER and HOR. We will start by looking at the Volmer reaction. Next we take the Heyrovsky reaction and finally the results for the Tafel reaction are presented. As we conclude that the Tafel reaction is most likely the rate-determining step for both HER and HOR, we consider that reaction in more detail when we calculate the activation energies and the exchange currents. Then we consider the structure dependence of different facets of the Pt crystal. After that, a range of different metals and facets is discussed. Finally, we use all the DFT calculated values in a kinetic model where we construct a volcano for HER and HOR.

3.1. Elementary Reaction Steps on Pt(111). ***3.1.1. Volmer Reaction.*** In the initial step of HER, the Volmer step,

$$H^+ + e^- \rightarrow H^*$$

an electron and a proton recombine to form adsorbed H on the surface. Being a charge transfer reaction, it requires some special considerations. First of all, the full electrochemical double layer setup, including a water bilayer outside the metal surface, is needed in order to accurately treat the solvation of the proton and to account for the extra charge in the slab. Second, we use the extrapolation scheme presented above and we report all energies at different absolute electrode potentials in the limit where the potential does not change during the reaction (cf. Figure 4c,d).

Reaction and activation energies have been extracted at five different proton concentrations: $\theta_{H^*} = 1/6$, 1/12, 1/18, 1/24, and 0. We also vary the H coverage on the surface to obtain self-consistency between the electrode potential and the H coverage according to Figure 6 or any cyclic voltammogram on Pt(111).[3] In the following we will only use systems having the right correspondence between H coverage and U, except when considering the activation barrier as a function of reaction energy where we include all the data for completeness.

Figure 7 shows the activation barrier for the Volmer reaction, both in the HER and the HOR direction, as a function of the reaction energy and the electrode potential. In all cases the dependence is essentially linear. The linear relation between E_a and ΔE observed in Figure 7 for the electrochemical processes is well-known in gas-phase/solid-state heterogeneous catalysis as a Brønsted−Evans−Polanyi (BEP) relationship[48−52] and also generally in chemistry.[53] For the HER direction, the energy

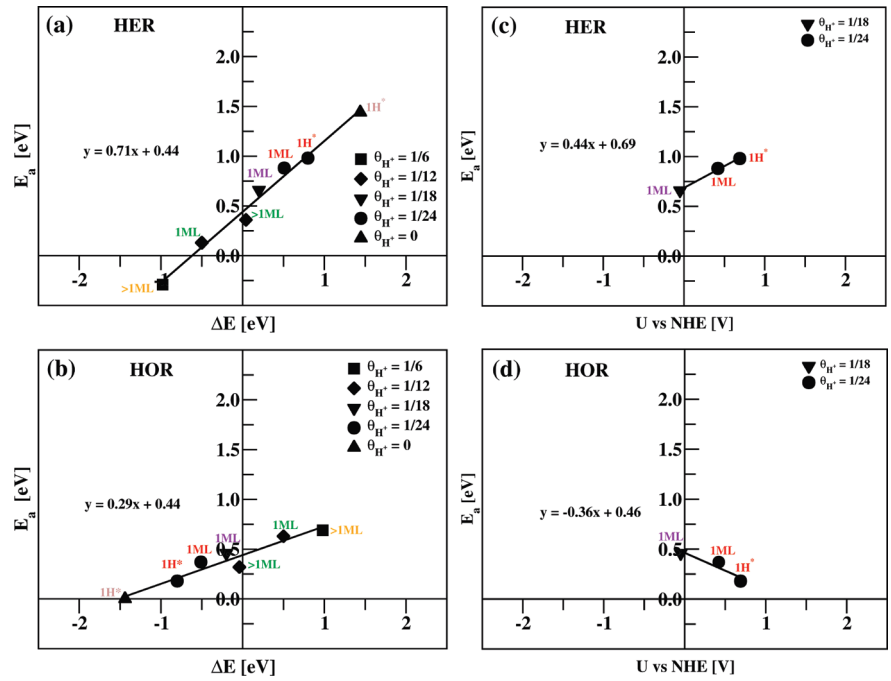

Figure 7. Activation barriers, E_a, for the Volmer step in (a and c) the HER ($H^+ + e^- \rightarrow H^*$) and (b and d) the HOR ($H^* \rightarrow H^+ + e^-$) as a function of (a and b) the reaction energy, ΔE, and (c and d) the electrode potential, U vs NHE, on the Pt(111) electrode. $\chi^2 = 0.03$ (a), 0.03 (b), 0.00 (c), and 0.01 (d).

barrier is 0.44 eV at $\Delta E = 0$ and 0.69 eV at $U = 0$ V vs NHE. For HOR direction, the energy barrier is also 0.44 eV at $\Delta E = 0$ and 0.46 eV at $U = 0$ V vs NHE. The 0.23 eV difference between the barrier heights for HER and HOR at $U = 0$ V (equilibrium) is due to the difference in the reaction energies for those two reactions.

If we assume a normal prefactor, 10^{13} site^{-1} s^{-1}, for the Volmer reaction, as we obtained from our calculations for the Heyrovsky reaction,[11] the rate of the Volmer reaction will be very high around $U = 0$, in agreement with experiments.[2] We will show later that other elementary steps in the HER/HOR have larger barriers at $U = 0$, and conclude from our first-principles calculations that the Volmer reaction can be treated as being in equilibrium at room temperature during HER/HOR and the coverage of H on the surface is given by the chemical potential of hydrogen, or the electrode potential.

3.1.2. Heyrovsky Reaction. In the final step of the HER, two possibilities for desorbing H_2 are available: the Tafel reaction or the Heyrovsky reaction. We start with the Heyrovsky reaction:

$$H^* + H^+ + e^- \rightarrow H_2$$

where a solvated proton from the electrolyte reacts with an adsorbed H and an electron from the surface to form the H_2 molecule. Since this is also a charge transfer reaction, an accurate analysis of the energetics requires the double layer model and the extrapolation scheme previously applied to the Volmer reaction. Using the information obtained in Figure 4a,b when both the reaction energies and activation energies have been extrapolated to $\Delta U = 0$, we can now plot the extrapolated activation energies against the extrapolated reaction energies as shown in Figure 8 for HER and HOR, respectively, on Pt(111). The proton concentration, θ_{H+}, in the water bilayer has been varied and so has the H coverage on the surface, from having slightly more than 1 ML on the surface to having very low coverage (or 1 H* in a super cell). The relation between the activation energy and the reaction energy is clearly linear with an intercept at $\Delta E = 0$ of 1.03 eV for both reactions. The intercept is slightly higher here than what we reported in ref 11, where it was 0.86 eV. Besides the fact that we are including more variation in proton concentration and especially the H coverage, we have applied the extrapolation scheme so both the activation barriers and the reaction energies are extrapolated to $\Delta U = 0$. Another important difference is that now all the activation barriers are calculated via the NEB method whereas we made a less detailed approximation for the TS in the earlier work.

In Figure 8 (right) we include the activation barriers for HER and HOR versus the electrode potential, obtained from the WF of the systems and with our internal measure of the electrode potential as discussed in section 2.2. As for the Volmer reaction above we attempt to have a H coverage on the surface that is consistent with the potential. Here we have obtained a semi-quantitative agreement between the H coverage and the potential with both experimental CVs[3] and our theoretical CVs.[32] The activation barrier for HOR is around 0.8 eV at $U = 0$ V vs NHE, whereas it is around 1.4 eV at $U = 0$ for HER. As for the Volmer reaction, the difference between the HER and the HOR barriers is coming from the reaction energies. Our analysis indicates that the Heyrovsky reaction should be very slow on the Pt(111) surface at $U = 0$ V. At extremely high overpotentials, around -1 V for HER and $+0.5$ V for HOR, the barrier for the Heyrovsky reaction becomes much lower or around 0.3 eV. The size of the overpotential seems to be somewhat greater here than in the study by Wang et al.[12] in which they conclude that the Volmer−Heyrovsky route becomes important for HOR at around $+0.25$ V vs NHE. These results are in qualitative agreement though.

3.1.3. Tafel Reaction. The other possible elementary step for evolving H_2 in HER (or dissociating H_2 in HOR) is the Tafel reaction:

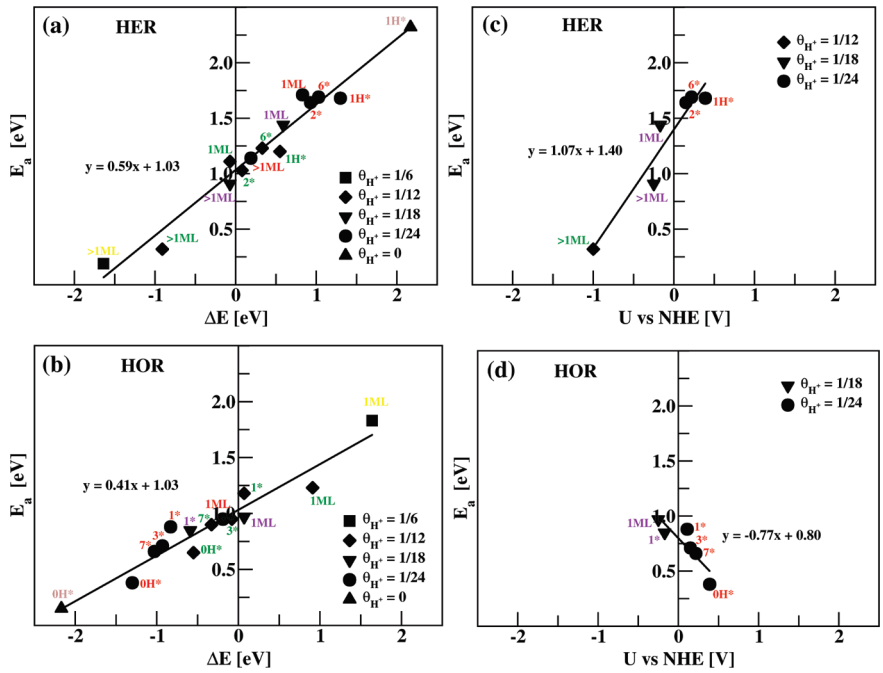

Figure 8. Activation barrier for (a and c) the HER and (b and d) the HOR on Pt(111) via the Heyrovsky reaction as a function of (a and b) the reaction energy, ΔE, and (c and d) the electrode potential, U vs NHE. $\chi^2 = 0.15$ (a), 0.16 (b), 0.13 (c), and 0.05 (d).

$$2H^* \leftrightarrow H_2 + 2^*$$

Since the Tafel reaction is a homolytic reaction (a Langmuir−Hinshelwood type reaction) it is not necessary to explicitly include water, ions, electric potentials, or electric fields[11] in order to describe it in an electrochemical environment. It should be noted that Gohda et al. calculated a 0.17 eV increase in activation energy when including water in the simulations of the Tafel reaction in the HOR direction[54] whereas we find negligible difference for the Tafel reaction in the HER direction.[11] This increase in barrier height when including water is not coming from the weak water-induced modification of the electronic structure of Pt(111). It is due to the interaction of H_2 with the water when H_2 propagates through the water layer.[54] The effect of water on the energetics of HER and HOR is thus a surface-independent parameter.

Avoiding inclusion of water simplifies the DFT calculations enormously as only a surface slab and adsorbed hydrogen have to be included in the model. However, as mentioned above, the coverage is a function of the potential and the coverage will affect the Tafel reaction. In this indirect way the electrochemical potential is playing a role.

In Figure 9a we have plotted the activation energies, E_a, against the reaction energies, ΔE, in both the HER and the HOR directions on Pt(111). The variation in both E_a and ΔE is due to differences in H coverage. E_a and ΔE are linearly correlated, following the BEP relationship. The slope is 0.45 for HER and 0.55 for HOR and the intercept is 0.55 eV for both directions. This is a considerably lower activation energy than obtained for the Heyrovsky reaction at $\Delta E = 0$, where it is 1.03 eV. This strongly indicates that the Tafel reaction is much faster than the Heyrovsky and the predominant mechanism on Pt(111).

Using Figure 6, and eq 8 the H adsorption free energy scale can be converted into a potential scale vs NHE as shown in Figure 9b. It is seen that for the U-values of interest when considering HER, i.e., just below 0 V vs NHE, the activation barriers are around 0.85 eV. Figure 9b shows the corresponding barriers for the Tafel reaction in the HOR direction. At positive potentials the activation barriers are low, 0.2−0.3 eV, whereas getting closer to $U = 0$ V the barriers start to increase and are around 0.4−0.6 eV. This is due to the fact that in the small unit cells (2 × 2) we are using, all those calculations have only one empty site on the surface and when dissociating H_2, the on-top sites become occupied which are high in energy, as we saw in Figure 6 above 1 ML. If we now introduce a dimer vacancy in a bigger unit cell (4 × 4) where we have an initial H coverage of 14/16 ML and we dissociate H_2 to end up with 1 ML on the surface, the barrier decreases at $U = 0$ V to 0.4 eV (open square in Figure 9b). One could actually have a triple vacancy and get even lower barriers according to studies on the Pd(111) surface[55−57] but the probability of creating empty sites and the aggregation energy would affect the total rate in the end. We will analyze this further in the next section.

The barriers for the Tafel reaction for HER around 0.85 eV and HOR around 0.4 eV at $U = 0$ V are considerably lower than the ones for the Heyrovsky reaction at $U = 0$ V (1.4 eV for HER and 0.8 eV for HOR). The barrier for the Tafel reaction is also lower than the Heyrovsky reaction barrier for the whole potential region from −1 to +0.5 V. At these extremes in potentials, the barriers for the Heyrovsky and Tafel reactions become, however, somewhat similar in size.

The activation barrier of 0.85 eV for the Tafel reaction in the HER direction is higher than the one for the Volmer step at $U = 0$ V (0.69 eV for HER). The barriers for the Tafel and the Volmer reactions are, however, similar in the HOR direction, 0.4 and 0.46 eV, respectively. Our results indicate that the Volmer−Tafel route is the predominant mechanism for both HER and HOR on Pt(111) at $U = 0$ V. Thus, we can focus on the Tafel reaction when analyzing the kinetics further and when considering other metal surfaces, facets, and steps. Before we analyze the Tafel reaction in detail we construct a free energy diagram of all the elementary steps in the next section.

3.1.4. Standard Free Energy Diagram. To construct an overall picture of the energetics of the three elementary reaction steps—Volmer, Heyrovsky, and Tafel—a standard free energy diagram (FED) is constructed in Figure 10. We define this as a *standard free energy* since there is no configurational part of

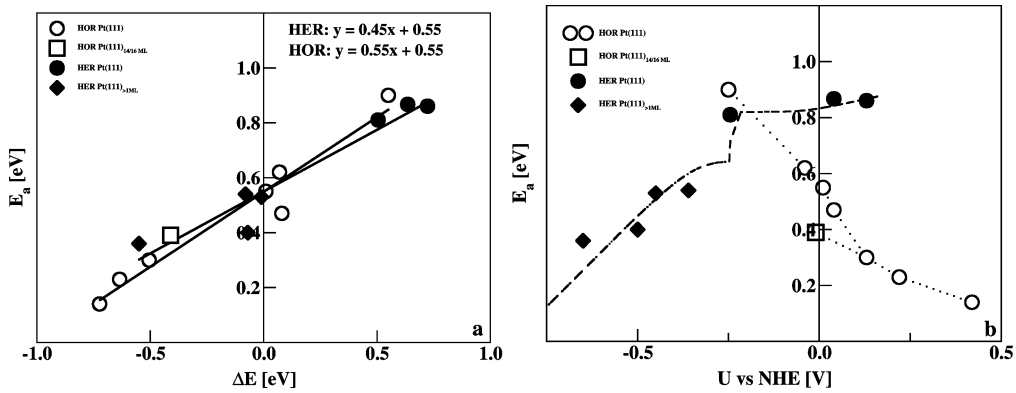

Figure 9. Activation barrier, E_a, for HER and HOR on Pt(111) via the Tafel reaction as a function of (a) the reaction energy, ΔE, and (b) the electrode potential, U. $\chi^2 = 0.02$ for both HER and HOR in part a.

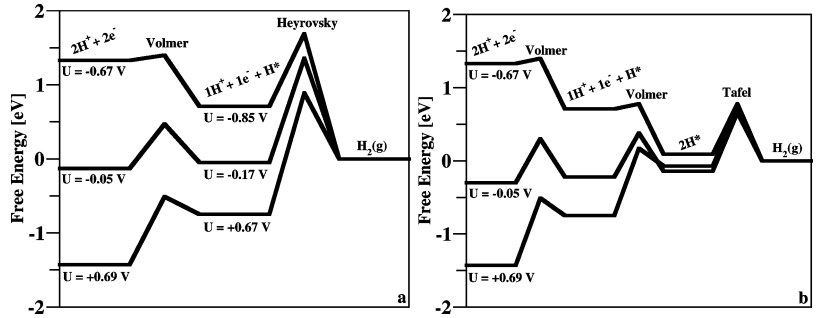

Figure 10. Standard free energy diagram for the Volmer−Heyrovsky route (a) and Volmer−Tafel route (b) on Pt(111). The electric potential, U, deduced from the WF is given for each free energy level.

the entropy included. Hence all the free energy states in Figure 10 are at a fixed H* coverage. For the Volmer and the Heyrovsky steps we have picked out the three systems closest to zero electrode potential from Figure 5. It should be noted that here the analysis becomes more transparent if we add together the reaction free energies of the Volmer and Heyrovsky steps. It is equivalent to adding the negative of the two individual electrode potentials, since the H* energy cancels out. It is obvious from Figure 10 that while the Heyrovsky state ($1H^+ + 1e^- + H^*$) changes by $1U$ plus the H adsorption energy, the Volmer state ($2H^+ + 2e^-$) changes by $2U$ from the H_2 state. These explicit DFT calculations show how the chemical potential, μ, is related to the electric potential, U, via the following simple equation: $\mu = -eU$, where e is the transferred charge. It is noted here that if the configurational part of the entropy had been included, all the free energy levels would be in equilibrium, and have the same free energy value.

In Figure 10a the extrapolated activation free energy barriers for the Volmer and the Heyrovsky reactions, obtained from Figure 4d,b, are also included. (The ZPE of the TS structure is calculated via NMA DFT calculations to be 0.20 eV for the Volmer TS and 0.26 eV for the Heyrovsky TS. The entropy terms have been neglected as explained elsewhere.[21]) It is evident while the activation barriers are quite low for the Volmer reaction they are very high for the Heyrovsky reaction. For comparison the activation free energy barriers of the Volmer−Tafel route have been included in Figure 10b. The barrier for the Tafel reaction is approximately half as high as the barrier for the Heyrovsky reaction, whereas it is only slightly higher than the barrier for the Volmer reaction. Thereby, we conclude that the Volmer step is the fastest step of these elementary steps and the Tafel step is the rate-determining step.

3.2. Detailed Analysis on the Kinetics of the Tafel Reaction on Pt(111). The calculations we have performed for the activation energy as a function of H coverage for the Tafel reaction on Pt(111) can be considered as the mean field solution to the problem. Here we will present more elaborate analysis of the kinetics of HER and HOR on Pt(111). Instead of assigning each activation barrier to a given H coverage, we will associate an activation barrier to each configuration described by the number of H nearest neighbors (NN). In Table 1 we show the barriers and reaction energies for HER and HOR from Figure 9a as a function of the NN configuration. We use the convention that NN is for the FS for HOR and hence for the IS for HER. These are the states determining the actual heights of the barriers. We have chosen to only consider data for 1 ML H coverage or less, since we will mainly be interested in potential around $U = 0$ V vs NHE where the coverage on Pt(111) does not exceed 1 ML, cf. Figure 6.

TABLE 1: Tafel (HER/HOR) Activation Energies, E_a, and Reaction Energies, dE, at Different Nearest-Neighbor (NN) Configurations[a]

HOR FS nn/HER IS nn	E_a^{HOR}	dE^{HOR}	E_a^{HER}
0	0.14	−0.72	0.86
1	0.14	−0.72	0.86
2	0.23	−0.64	0.87
3(*)	0.25	−0.60	0.85
4(*)	0.27	−0.56	0.83
5	0.30	−0.51	0.81
6	0.39	−0.41	0.80

[a] All energies are in eV/H_2. For the NN configuration marked (*) a linear interpolation has been taken for the E_a and dE from NN = 2 and 5.

In Figure 11 we have calculated the probability of having a given nearest neighbor (NN) configuration at certain H coverages from 0 to 1 ML, both with an interacting lattice model using Metropolis Monte Carlo (MC) simulations and analytically with a noninteracting lattice model. For the MC simulation a hexagonal FCC(111) surface is modeled with a simple lattice

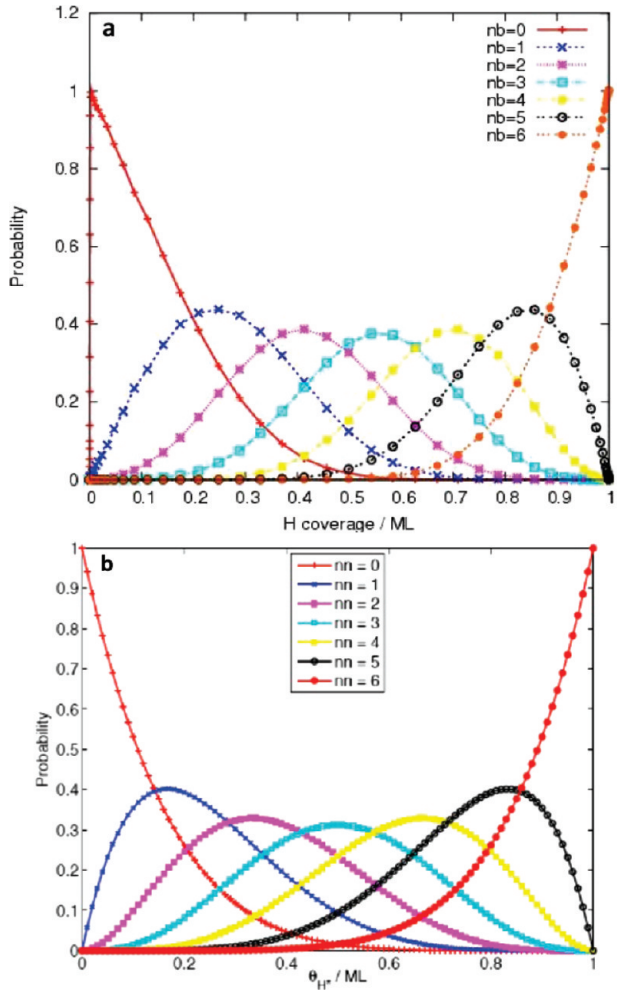

Figure 11. Probability of having a given nearest neighbor (NN) configuration at varying H coverage, calculated with (a) Metropolis Monte Carlo and (b) analytically.

model where each H in the FCC site can interact with up to 6 nearest neighbors. The analytical hexagonal lattice model is noninteracting and is given by the binomial coefficients

$$P_i(\theta) = \binom{6}{i}\theta^i(1-\theta)^{6-i} \tag{9}$$

As can be seen from Figure 11, the MC simulation (including interactions) does not deviate much from the noninteracting analytical model. We therefore use the analytical model in the following analysis since it is more transparent.

The Tafel HER rate is given by θ^2 times a sum over weighted (with $P_i(\theta)$ in eq 9) rate constants $k_{T,i}^{HER} = \nu * \exp(-E_{a,i}^{HER}/k_BT)$. We use the approximate attempt frequency, $\nu = 10^{13}$ site^{-1} s^{-1}, as the prefactor, which we found to agree well with the measured absolute rate for HER when used together with our calculated activation barriers.[11] The activation energies $E_{a,i}^{HER}$ are given in Table 1. We get the rate equation

$$r_T^{HER}(\theta) = \theta^2 \sum_{i=0}^{6} P_i(\theta) k_{T,i}^{HER} \tag{10}$$

With the expression for $P_i(\theta)$ in eq 9 inserted into eq 10 we end up with the following expression for the Tafel HER rate:

$$r_T^{HER}(\theta) - \nu \sum_{i=0}^{6} \binom{6}{i}\theta^{i+2}(1-\theta)^{6-i} \exp(-E_{a,i}^{HER}/k_BT) \tag{11}$$

The corresponding expression for the HOR rate can be written as

$$r_T^{HER}(\theta) = \nu \exp(\Delta S/k_B) \sum_{i=0}^{6} \binom{6}{i}\theta^{i}(1-\theta)^{8-i} \exp(-E_{a,i}^{HER}/k_BT) \tag{12}$$

where $\Delta S/k_B = -15.86 \rightarrow \exp(\Delta S/k_B) = 1.3 \times 10^{-7}$ is the entropic barrier or loss of entropy when H_2 comes from the gas phase and dissociates on the surface, $-T\Delta S = 0.41$ eV at standard conditions.

For a given H coverage we calculate the rate of both the HER and the HOR using eqs 11 and 12. In Figure 12 the result is shown as a function of the H coverage at 300 K. At equilibrium, the rates for HER and HOR are the same and there is no net flow of current. This corresponds to $U = 0$ V vs NHE at standard conditions and where the H coverage is 0.87 ML. This can be compared to the value 0.86 ML obtained with another approach in Figure 6.

At equilibrium, the exchange rate is 0.21 site^{-1} s^{-1} at 300 K. By changing units we get $i_0 = 5.1 \times 10^{-5}$ A cm^{-2} for the exchange current density. This is to be compared with the experimental value for the exchange current density on Pt(111) at 303 K, $i_0 = 4.5 \times 10^{-4}$ A cm^{-2}.[2]

Here we show that our calculated barrier for the Tafel reaction gives a similar rate as experiments on the same surface. However, experimentally the activation barrier obtained from Arrhenius type analysis is around 0.2 eV for HER and HOR on Pt(111).[2] This corresponds to a prefactor on the order of 10^3 site^{-1} s^{-1}, or 10 orders of magnitude lower than a normal prefactor. We are presently not able to explain these experimental data.

3.3. Structure Dependence over Pt(111), Pt(100), and Pt(110). In the following section we discuss the HER and HOR rates for different facets of Pt and compare it with experiments by Markovic et al.[2] First we study the heat of adsorption vs coverage. Then we compare the calculated rates obtained solely from the Tafel activation barriers with the measured ones. We

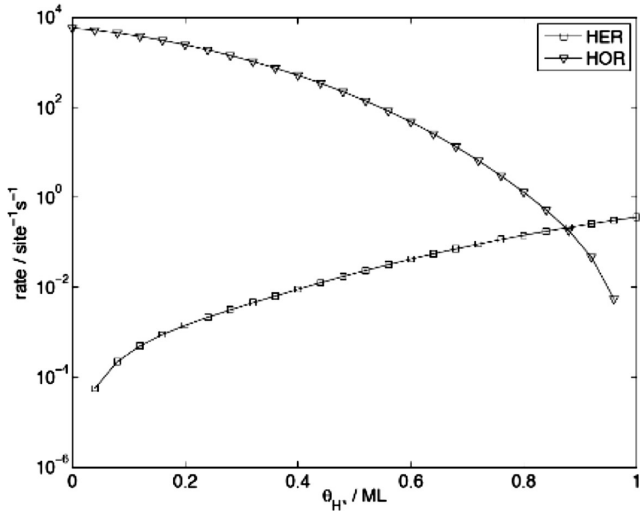

Figure 12. Total Tafel HER and HOR rates at 300 K, plotted vs the H coverage.

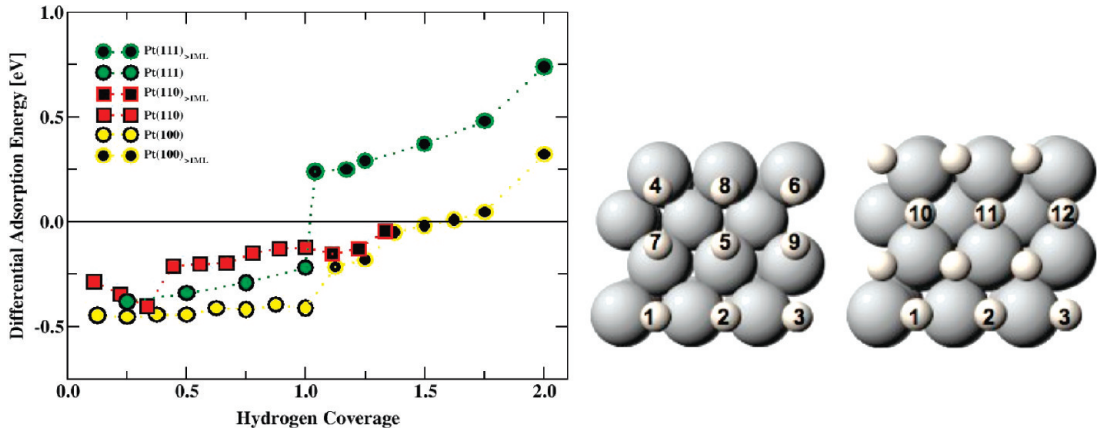

Figure 13. Differential H adsorption energy as a function of H coverage for the three most stable crystal facets of Pt: the (111), (110), and (100) facets. For convenience, we have made the symbols black in the middle when exceeding 1 ML. The atomic structures show the order of H adsorption on the Pt(110) surface. When exceeding 1 ML H coverage (where 1 ML is defined as 9 H adatoms on 9 Pt surface atoms) a conformational change is observed where atoms labeled 4−9 diffuse slightly away from the valley to create space for atoms labeled 10−12 to adsorb on the surface.

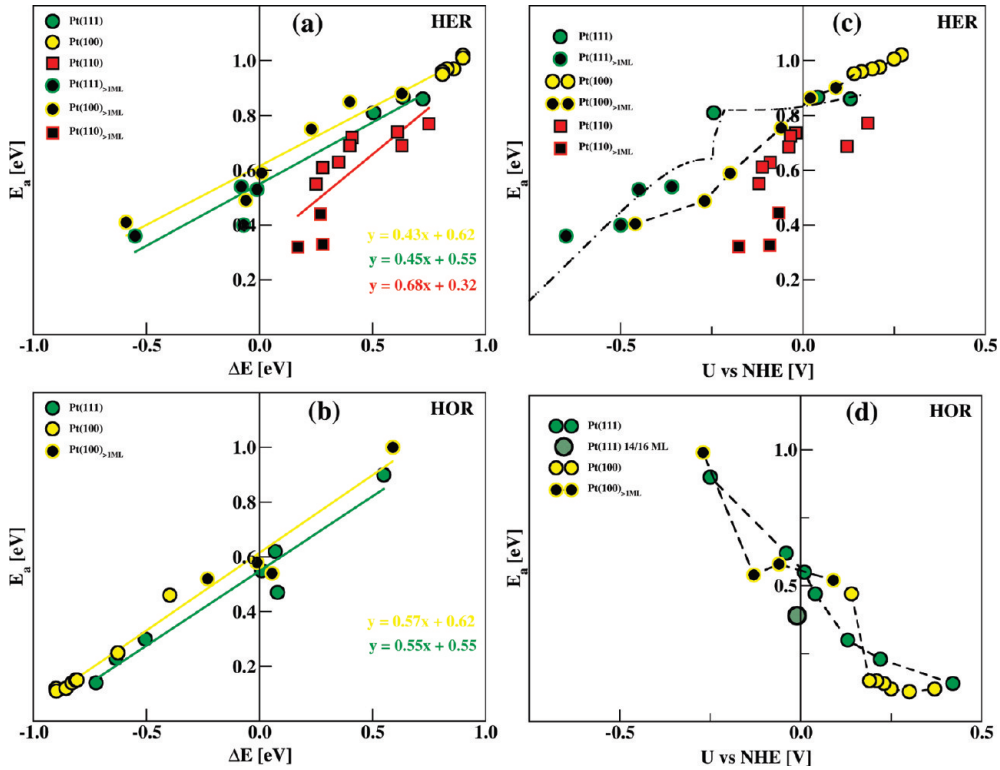

Figure 14. Activation barrier for the HER (a and c) and the HOR (b and d) on Pt(111) and Pt(100) and for the HER (a and c) on Pt(110) via the Tafel reaction as a function of the reaction energy (a and b) and the electrode potential, U vs NHE (c and d). $\chi^2 = 0.02$ for Pt(111) (a and b), 0.02 for Pt(100) (a and b), and 0.10 for Pt(110) (a).

will assume that the Volmer reaction is in equilibrium on all facets as generally found in experiments.[3] We will assume that the Heyrovsky pathway is not active on any of these surfaces since our calculations on the Pt(111) electrode show that it is so far from active that the relatively small difference that we find in energetics between the different facets cannot change that picture.

3.3.1. Heat of Adsorption. In Figure 13 we report the differential adsorption energy (eq 4) as a function of H coverage for the Pt (111), (110), and (100) facets. As before, H occupies FCC sites up to 1 ML and on-top sites above 1 ML on the (111) facet. On the (100) facet, however, it adsorbs on the bridge sites all the way up to 2 ML.

The Pt(110) electrode was modeled with a missing row reconstruction in accord with experimental observations under electrochemical conditions.[3] The first hydrogen atoms prefer to bind to the rim of the outermost Pt row. After those states have been filled, we find that it is most favorable for H to adsorb on-top the Pt atoms next to the rim. This is in agreement with recent experimental and theoretical work on the Pt(110) surface[58] but in contrast to theoretical work on Ni(110) and Pd(110) where the adsorption instead starts on the (111) microfacet.[59,60] When all the surface atoms have been covered (at 1 ML) the next H to be adsorbed prefers to bind on bridge sites down in the valley.

The discontinuity in the energy profile when going beyond 1 ML is much less pronounced on Pt(100) than on Pt(111) and it is more or less smeared out on the rough Pt(110) surface. The effect this will have on the Tafel reaction when H_2 desorbs from these different facets or dissociates on them at varying H coverage (or electrode potential) is investigated below.

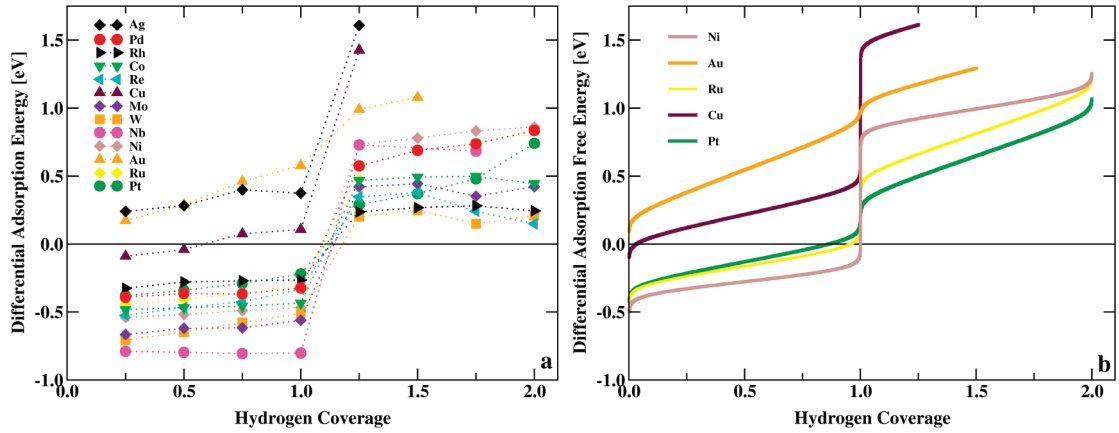

Figure 15. (a) Differential energy of H adsorption on close-packed metals. (b) Differential free energy of H adsorption on a few closed-packed metals.

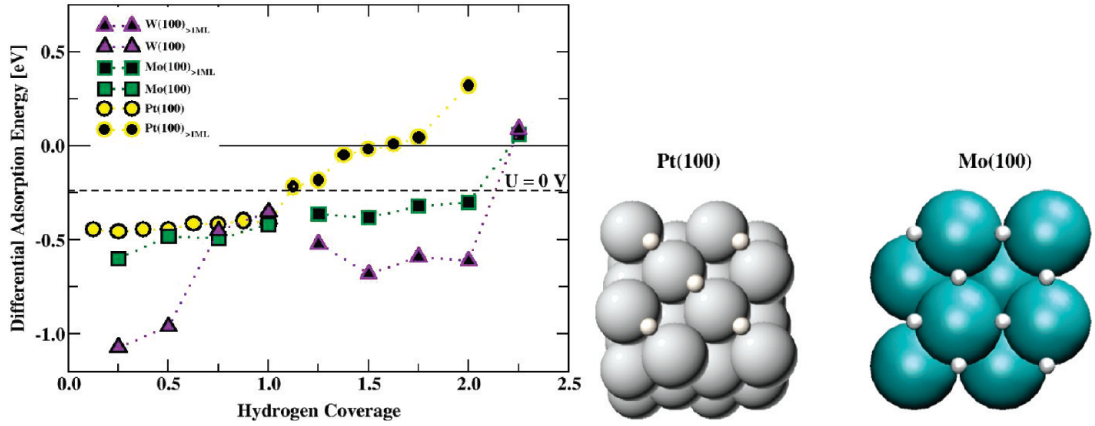

Figure 16. Differential energy of H adsorption on open surfaces. The atomic structures show Pt(100) and Mo(100) surfaces with 1 and 2 ML of H adatoms, respectively.

3.3.2. Tafel Reaction. In Figure 14 we have calculated activation barriers for HER and HOR via the Tafel reaction on Pt(111) and Pt(100) and for HER on Pt(110). We vary the H coverage, which gives us both variations in the reaction energy and in the electrode potential. We assume that the prefactors are the same for all the facets. That allows us to compare our calculated rates to the measured rates for these facets which we do because the measured activation barriers coming from the Arrhenius analysis are all around 0.1−0.2 eV for these facets,[2] or much lower than our HER barriers (around 0.8 eV) at $U = 0$.

In the following we will calculate the HER rates for the different facets at $U = 0$ V vs NHE. The HER barriers on the (111) and (100) are both around 0.85 eV at $U = 0$ V, whereas the barrier on the (110) facet is around 0.74 eV at $U = 0$ V. Since for these facets every activation barrier is calculated for only one particular H coverage, we use our elaborate analysis from section 3.2 for the Pt(111) facet as a starting point when comparing the facets. Since Pt(111) and Pt(100) have the same activation barriers at $U = 0$ (Figure 14c) the Pt(100) facet has the same exchange current as Pt(111), or $i_0 = 5.1 \times 10^{-5}$ A cm^{-2} (calculated in section 3.2). This is in agreement with the measured ones, 6.0×10^{-4} A cm^{-2} for Pt(100) and 4.5×10^{-4} A cm^{-2} for Pt(111), at 303 K.[2] From the difference in activation barriers between Pt(111) and Pt(110) we calculate $i_0 = 3.7 \times 10^{-3}$ A cm^{-2} for Pt(110) in good agreement with the measured one, 9.8×10^{-4} A cm^{-2}, on Pt(110).[2]

We see similar structure dependence on the rates as Markovic et al.[2] and our absolute values are in quite good agreement with their measured ones. However, our activation barriers do not agree with the experimental ones obtained via Arrhenius analysis. We calculate around 0.74−0.85 eV at $U = 0$ V whereas their values are around 0.1−0.2 eV.

3.4. Heat of Adsorption on Other Electrodes. In this section we will consider other metals, both in their close-packed structures and other facets and steps. This includes Au, Ag, Cu, Pt, Pd, Ni, Ir, Rh, Co, Ru, Re, W, Mo, and Nb. First we calculate the H adsorption energy and free energy on these different metal surfaces. Then we calculate the rate of the Tafel reaction on the complete range of surfaces.

3.4.1. Close-Packed Surfaces. Figure 15a shows the calculated differential H adsorption energies for a range of close-packed transition metals. In Figure 15b the free energy profile, calculated via eq 5, at 300 K for Ni, Au, Ru, Cu, and Pt is shown. On the close-packed surfaces, H is adsorbed in 3-fold FCC sites up to a coverage of 1 ML. When exceeding 1 ML, additional H starts occupying on-top sites and there is a discontinuity in the energy profile. At room temperature, ΔG_{H^*} is negative on the more reactive metals (Nb, W, Mo, Ni, Re, and Co) as long as $\theta_{H^*} \leq 1$ ML, which means that these surfaces will be fully covered. On the less reactive metals, like Pt, the H coverage is on the other hand a bit less than 1 ML when $\Delta G_{H^*} = 0$. Finally, the H coverage on the inert metals (Cu, Ag, and Au) is very small at room temperature since $\Delta G_{H^*} > 0$ for all except the lowest coverage.

If we make the conversion of scales, i.e. changing ΔG_{H^*} to $-eU$, we find that the coverage will be about 1 ML at $U = 0$ V vs NHE on the most reactive metals, but very low on the

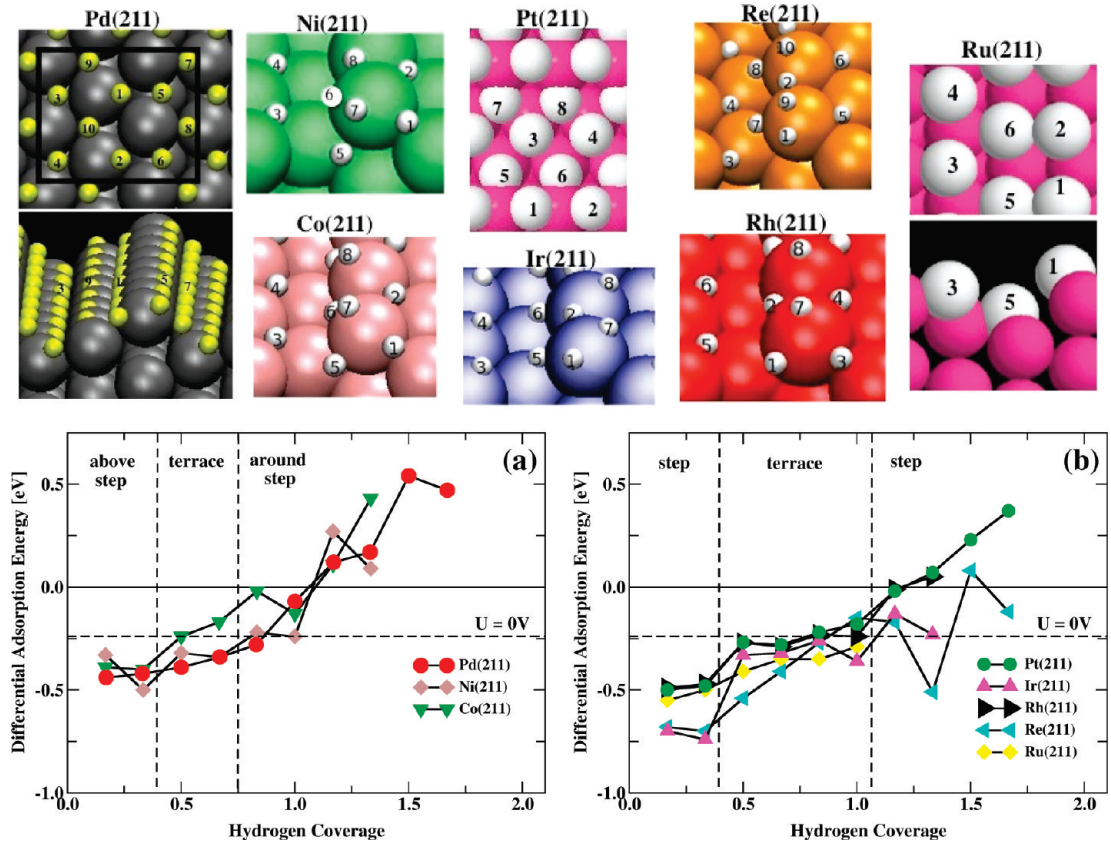

Figure 17. Differential energy of H adsorption on stepped surfaces. The atomic structures above show the order of H adsorption.

noble metals: Cu, Ag, and Au. For the noble metals a substantial negative bias is required in order to adsorb any appreciable amounts of H. We further notice that a coverage exceeding 1 ML could in principle be achieved on the reactive metals by decreasing U to approximately -0.5 to -0.8 V vs NHE. However, before that coverage is reached hydrogen molecules start forming on the surface via the Tafel reaction.

3.4.2. More Open Facets and Steps. Since polycrystalline surfaces and nanoparticles consist of different types of flat surfaces as well as steps, kinks, and other defects, it is interesting to calculate the heat of adsorption for more open facets than the close-packed ones. Here we have considered the FCC Pt(100) facet and the BCC W(100) and Mo(100) facets. A number of different adsorption sites are considered and the bridge sites are found to be the most stable ones. Since we have two bridge sites for each metal atom, we can fill the surface with bridge sites up to 2 ML. We discussed the Pt(100) results above in connection with Figure 13.

In Figure 16 we have included a line indicating $U = 0$ V vs NHE by applying eq 8 at standard conditions. The Pt(100) surface is able to adsorb slightly more than 1 ML according to this simple model. The more reactive Mo(100) and W(100) surfaces can both adsorb considerable more H on the surface than the Pt(100) surface. The Mo(100) surface will adsorb 2 ML of H at $U = 0$ V or fill all the bridge sites. Occupying the 4-fold site above 2 ML would require around -0.25 V in overpotential. A similar situation is on the W(100) as on the Mo(100), besides that at 2 ML, H adsorbs much stronger on W than on Mo. It should be noted that quite strong reconstruction occurred on the W(100) surface when adsorbing 0.75 and 1 ML.

To model the effect of the low-coordinated defect sites on a real catalyst, the (211) stepped surface is used. In Figure 17 we have calculated the H adsorption energy at different H coverage on a number of (211) metals. We have divided it into two sets of figures, where on the left we group Pd(211), Ni(211), and Co(211) together and on the right Pt(211), Ir(211), Re(211), and Rh(211). The metals are divided in the two groups based on the order in which the H atoms adsorb on the surface.

The general trend for all the metals is similar, however. The first H adsorb around the step, whereas the next H binds to the terrace. Around 1 ML (where 1 ML is defined here as 1 H per 1 surface metal atom), the next H binds to a new site around the (bottom of the) step. On these surfaces there is more space and more possibility of new adsorption sites, which leads to much smoother and more continuous adsorption curve behavior than at the close-packed surfaces, where filling up all the 3-fold sites means that only the on-top sites are available above 1 ML.

If we compare Pd(211) and Pt(211) the first H adsorbs on a 3-fold hollow site above the step on Pd(211) whereas the first H binds to the bridge site on the Pt(211) step. The tendency to occupy a 3-fold site is larger on Pd than on Pt where bridge to 3-fold energy differences are small, and H therefore easily moves to the bridge site to take full advantage of the high lying d-states at the step.

In Figure 17 a line for $U = 0$ V has been added as for the (100) metals in Figure 16. For most of the metals the steps have been occupied initially and the terrace has been filled with H at $U = 0$. This means that at $U = 0$, the close-packed structure is a sufficient model to capture the trends between the metals as we will discuss in the following section 3.5. This means that the activation barrier at the close-packed surface is what determines the HER reactivity of, e.g., a polycrystalline metal.

3.5. Trends in Exchange Currents for Different Metals: The Volcano Plot. The ability of a given metal to catalyze the HER (or HOR) is usually measured by the exchange current

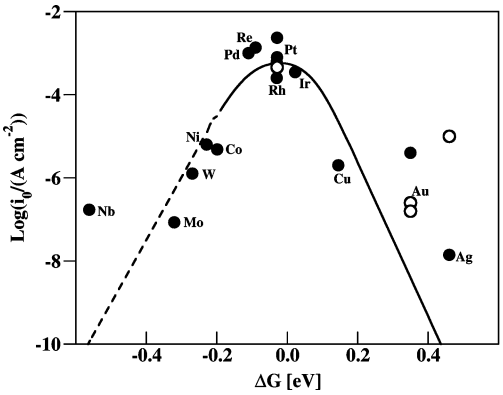

Figure 18. A volcano plot. The data points are measured exchange current density plotted versus the calculated free energy of H adsorption at $U = 0$ V. The metals on the left side of the volcano have high H coverage (1 ML) and the metals on the right side low H coverage (0.25 ML). The line is a prediction by a kinetic model in which all input parameters are taken from DFT calculations. The dashed line indicates that the metals which bind H stronger than 0.2 eV/H usually form oxides at $U = 0$ V. The open circles are (111) data whereas the filled circles are polycrystalline.

density, which is the rate of hydrogen evolution (or oxidation) per surface area at the potential where the reaction is at equilibrium ($U = 0$ V vs NHE at standard conditions). Different materials exhibit widely different exchange current densities. For over 50 years, it has been well established that if the exchange current density of the HER is plotted against some experimental measure of the metal hydrogen bond energy, a volcano-shaped curve is obtained.[61−65]

Recently, a simple and fast systematic approach that uses adsorption free energies calculated using DFT was introduced.[14] When the measured exchange currents of various metals were plotted against the calculated binding, the apex of the volcano appeared close to $\Delta G_{H^*} = 0$. Reference 14 also introduced a simple kinetic model of the exchange current, which reproduced the experimental data surprisingly well. Except for one free parameter, adjusting the overall magnitude of the volcano, the only input to this model was the calculated ΔG_{H^*}.

Here we employ a considerably more advanced kinetic model where all the parameters are obtained from the first-principle calculations presented in this work, i.e., no fitting parameter has been used. We assume the Volmer reaction to be in equilibrium as above. We discard the Heyrovsky reaction since it was concluded above that it is very slow on the Pt(111) electrode. The kinetics of the rate-limiting step found in this paper, the Tafel reaction, is used to get the overall magnitude and shape of the volcano plot, whereas in the simple kinetic model[14] the magnitude was modeled with a free adjustable parameter since there no activation barriers were included. The shape of the simple kinetic model was captured in ref 14 by assuming that the transfer coefficient is equal to one in the rate expressions. In the present study the activation barrier and its dependency on the reaction energy has been included, which describes the absolute rate and trends of the experiments extremely well, as discussed below.

In Figure 18 the experimentally measured exchange current density (same as in ref 14) is plotted against the H adsorption free energy, obtained with DFT calculations. For the metals on the left side of $\Delta G = 0$ we include high coverage (1 ML) since these metals will be filled with H at $U = 0$. For the metals on the right side, Cu, Au, and Ag, we use low H coverage (0.25 ML) in accordance with Figure 15b. In the volcano of ref 14 all ΔG_{H^*} were calculated at low H coverage (0.25 ML). Here, the data points fall nicely on a volcano-shaped curve as expected. The metals on the left side of the volcano may be oxidized (indicated by a dashed line). This means that presumably these are metal oxides and not the pure metals in these particular experiments. However, when the measured exchange current on these metal oxides is plotted as a function of the H binding free energy of the pure metal, it falls directly on the volcano, predicted from the present more advanced kinetic model.

To model this, we calculate the exchange current from eq 11. We assume that we can describe the variation in E_a with a BEP relation for Pt(111) from Figure 9a. The kinetic model agrees well with the experimental data and captures both the shape of the volcano and the absolute magnitude, although the latter is probably fortuitous given the accuracy of our calculations. We also note that in the detailed analysis of the Tafel reaction on Pt(111) in section 3.2 our calculated current was about an order of magnitude lower than what we have here. This is because for the construction of the volcano we use a BEP line for Pt(111) including H coverage above 1 ML in order to span more of the energy landscape. In section 3.2, however, we only included H coverage of 1 ML and less.

The good agreement throughout the metal series indicates that the Tafel barrier is the predominant and rate-limiting step on all metal electrodes.

4. Conclusions

Density functional theory results have been presented for the hydrogen oxidation reaction (HOR) and the hydrogen evolution reaction (HER) on a large number of transition metals with different surface structures.

On the basis of the calculated barriers, the BEP relationships for the three elementary mechanisms (Tafel, Heyrovsky, and Volmer) involved in the overall HOR and HER have been established. It is found that the predominant reaction mechanism on the Pt(111) electrode is the Tafel reaction. We calculate a barrier of around 0.85 eV at $U = 0$ V vs NHE, which is not in agreement with the experimental one of 0.2 eV. The exchange current we calculate from this barrier is, however, in perfect agreement with the same experiment.

We studied the structure dependence of different facets of Pt for the Tafel reaction. Our calculated rates are in good agreement with the rates observed experimentally for the same facets.

To gain further insight into the kinetics of the Tafel reaction, we considered different metals, different facets, and steps. Generally, the energetics follow a BEP relation that includes the Pt(111) data. Furthermore, the HER exchange current (current in the HER direction at $U = 0$ V vs NHE) has been evaluated for a range of hydrogen adsorption free energies, using a kinetic model that takes the full free energy landscape as input. The agreement with experimental data is excellent.

Acknowledgment. CAMD is funded by the Lundbeck Foundation. The Catalysis for Sustainable Energy initiative is funded by the Danish Ministry of Science, Technology and Innovation. This work was supported by the Danish Center for Scientific Computing, the Danish Council for Technology and Innovation's FTP program, the Strategic Electrochemistry Research Center, the Danish Research Councils (STVF), The Department of Energy, Basic Energy Sciences, the EU through the FC-Anode network, STREP no. NMP-2007-032175, and the MC-RTN network 'Hydrogen' and the Icelandic Science Foundation.

References and Notes

(1) *Hydrogen as a Future Energy Carrier*; Züttel, A., Borgschulte, A., Schlapback, L., Eds.; Wiley-VCH: Weinheim, Germany, 2008.

(2) Markovic, N. M.; Grgur, B. N.; Ross, P. N. *J. Phys. Chem. B* **1997**, *101*, 5405.
(3) Markovic, N. M.; Ross, P. N., Jr. *Surf. Sci. Rep.* **2002**, *45*, 117.
(4) Kunimatsu, K.; Senzaki, T.; Tsushima, M.; Osawa, M. *Chem. Phys. Lett.* **2005**, *401*, 451.
(5) Conway, B. E.; Jerkiewicz, G. *Electrochim. Acta* **2000**, *45*, 4075.
(6) Barber, J.; Morin, S.; Conway, B. E. *J. Electroanal. Chem.* **1998**, *446*, 125.
(7) Tavares, M. C.; Machado, S. A. S.; Mazo, L. H. *Electrochim. Acta* **2001**, *46*, 4359.
(8) Santana, J. A.; Mateo, J. J.; Ishikawa, Y. *J. Phys. Chem. C* **2010**, *114*, 4995.
(9) Cai, Y.; Anderson, A. B. *J. Phys. Chem. B* **2004**, *108*, 9829.
(10) Cai, Y.; Anderson, A. B.; Angus, J. C.; Kostadinov, L. N. *Electrochem. Solid-State Lett.* **2005**, *8*, E62.
(11) Skúlason, E.; Karlberg, G. S.; Rossmeisl, J.; Bligaard, T.; Greeley, J.; Jónsson, H.; Nørskov, J. K. *Phys. Chem. Chem. Phys.* **2007**, *9*, 3241.
(12) Wang, J. X.; Springer, T. E.; Adzic, R. R. *J. Electrochem. Soc.* **2006**, *153*, A1732.
(13) Rossmeisl, J.; Nørskov, J. K.; Taylor, C. D.; Janik, M. J.; Neurock, M. *J. Phys. Chem. B* **2006**, *110*, 21833.
(14) Nørskov, J. K.; Bligaard, T.; Logadottir, A.; Kitchin, J. R.; Chen, J. G.; Pandelov, S.; Stimming, U. *J. Electrochem. Soc.* **2005**, *152*, J23.
(15) Shubina, T. E.; Koper, M. T. M. *Electrochem. Commun.* **2006**, *8*, 703.
(16) Vassilev, P.; van Santen, R. A.; Koper, M. T. M. *J. Chem. Phys.* **2005**, *122*, 054701.
(17) Roudgar, A.; Groβ, A. *Chem. Phys. Lett.* **2005**, *409*, 157.
(18) Filhol, J. S.; Neurock, M. *Angew. Chem., Int. Ed.* **2006**, *45*, 402.
(19) Otani, M.; Sugino, O. *Phys. Rev. B* **2006**, *73*, 115407.
(20) Sugino, O.; Hamada, I.; Otani, M.; Morikawa, Y.; Ikeshoji, T.; Okamoto, Y. *Surf. Sci.* **2007**, *601*, 5237.
(21) Rossmeisl, J.; Skúlason, E.; Björketun, M. E.; Tripkovic, V.; Nørskov, J. K. *Chem. Phys. Lett.* **2008**, *466*, 68.
(22) Jinnouchi, R.; Anderson, A. B. *J. Phys. Chem. C* **2008**, *112*, 8747.
(23) Payne, M. C.; Teter, M. P.; Allan, D. C.; Arias, T. A.; Joannopoulos, J. D. *Rev. Mod. Phys.* **1992**, *64*, 1045.
(24) Kresse, G.; Furtmüller, J. *Comput. Mater. Sci.* **1996**, *6*, 15.
(25) Vanderbilt, D. *Phys. Rev. B* **1990**, *41*, 7892.
(26) Dacapo pseudopotential code, URL: https://wiki.fysik.dtu.dk/dacapo, Center for Atomic-scale Materials Design (CAMD), Technical University of Denmark, Lyngby.
(27) Hammer, B.; Hansen, L. B.; Nørskov, J. K. *Phys. Rev. B* **1999**, *59*, 7413.
(28) Kresse, G.; Hafner, J. *Phys. Rev. B* **1993**, *48*, 13115.
(29) Kresse, G.; Furthmüller, J. *Phys. Rev. B* **1996**, *54*, 11169.
(30) Jónsson, H.; Mills, G.; Jacobsen, K. W. In *Classical and Quantum Dynamics in Condensed Phase Simulations*; Berne, B. J., Ciccotti, G., Coker, D. F., Eds.; World Scientific: Singapore, 1998.
(31) Henkelman, G.; Jónsson, H. *J. Chem. Phys.* **2000**, *113*, 9978.
(32) Karlberg, G. S.; Jaramillo, T. F.; Skúlason, E.; Rossmeisl, J.; Bligaard, T.; Nørskov, J. K. *Phys. Rev. Lett.* **2007**, *99*, 126101.
(33) Zundel, G.; Metzger, H. *Z. Phys. Chem. (N.F.)* **1968**, *58*, 225.
(34) Zundel, G. In *The Hydrogen Bond-Recent Developments in Theory and Experiments. II. Structure and Spectroscopy*; Schuster, P., Zundel, G., Sandorfy, C., Eds.; North-Holland: Amsterdam, The Netherlands, 1976; pp 683−766.
(35) Wicke, E.; Eigen, M.; Ackermann, Th. *Z. Phys. Chem. (N.F.)* **1954**, *1*, 340.
(36) Eigen, M. *Angew. Chem., Int. Ed.* **1964**, *3*, 1.
(37) Marx, D.; Tuckerman, M. E.; Hutter, J.; Parrinello, M. *Nature* **1999**, *397*, 601.
(38) Randles, J. E. B. *Trans. Faraday Soc.* **1956**, *52*, 1573.
(39) Kötz, E. R.; Neff, H.; Müller, K. *J. Electroanal. Chem.* **1986**, *215*, 331.
(40) Schnur, S.; Groβ, A. *New J. Phys.* **2009**, *409*, 157.
(41) Haq, S.; Clay, C.; Darling, G. R.; Zimbitas, G.; Hodgson, A. *Phys. Rev. B* **2006**, *73*, 115414.
(42) Pajkossy, T.; Kolb, D. M. *Electrochim. Acta* **2001**, *46*, 3063.
(43) Nørskov, J. K.; Rossmeisl, J.; Logadóttir, Á.; Lindqvist, L.; Kitchin, J. R.; Bligaard, T.; Jónsson, H. *J. Phys. Chem. B* **2004**, *108*, 17886.
(44) Greeley, J.; Mavrikakis, M. *J. Phys. Chem. B* **2005**, *109*, 3460.
(45) Atkins, P. W., *Physical Chemistry*, 6th ed.; Oxford University Press: Oxford, UK, 1998; p 582.
(46) Atkins, P. W. *Physical Chemistry*, 6th ed.; Oxford University Press: Oxford, UK, 1998; pp 485, 925, and 942.
(47) Strmcnik, D.; van der Vliet, D.; Stamenkovic, V.; Markovic, N. M. *Electrochem. Commun.* **2008**, *10*, 1602.
(48) Nørskov, J. K.; Bligaard, T.; Logadottir, A.; Bahn, S.; Bollinger, M.; Hansen, L. B.; Bengaard, H.; Hammer, B.; Sljivancanin, Z.; Mavrikakis, M.; Xu, Y.; Dahl, S.; Jacobsen, C. J. H. *J. Catal.* **2002**, *209*, 275.
(49) Pallasana, V.; Neurock, M. *J. Catal.* **2000**, *191*, 301.
(50) Liu, Z. P.; Hu, P. *J. Chem. Phys.* **2001**, *114*, 8244.
(51) Logadottir, A.; Rod, T. H.; Nørskov, J. K.; Hammer, B.; Dahl, S.; Jacobsen, C. J. H. *J. Catal.* **2001**, *197*, 229.
(52) Ferrin, P.; Simonetti, D.; Kandoi, S.; Kunkes, E.; Dumesic, J. A.; Nørskov, J. K.; Mavrikakis, M. *J. Am. Chem. Soc.* **2009**, *131*, 5809.
(53) Hammett, L. P.; Paul, M. A. *J. Am. Chem. Soc.* **1934**, *56*, 830.
(54) Gohda, Y.; Schnur, S.; Groβ, A. *Faraday Discuss.* **2008**, *140*, 233.
(55) Mitsui, T.; Rose, M. K.; Fomin, E.; Ogletree, D. F.; Salmeron, M. *Nature* **2003**, *422*, 705.
(56) Lopez, N.; Lodziana, Z.; Illas, F.; Salmeron, M. *Phys. Rev. Lett.* **2004**, *93*, 146103.
(57) Groβ, A.; Dianat, A. *Phys. Rev. Lett.* **2007**, *98*, 206107.
(58) Minca, M.; Penner, S.; Loerting, T.; Menzel, A.; Bertel, E.; Zucca, R.; Redinger, J. *Top. Catal.* **2007**, *46*, 161.
(59) Kresse, G.; Hafner, J. *Surf. Sci.* **2000**, *459*, 287.
(60) Dong, W.; Ledentu, V.; Sautet, P.; Eichler, E.; Hafner, J. *Surf. Sci.* **1998**, *411*, 123.
(61) Gerischer, H. *Z. Phys. Chem. (N.F.)* **1956**, *8*, 137.
(62) Parsons, R. *Trans. Faraday Soc.* **1958**, *54*, 1053.
(63) Krishtalik, L. *Adv. Electrochem. Electrochem. Eng.* **1970**, *7*, 283.
(64) Trasatti, S. *J. Electroanal. Chem. Interfacial Electrochem.* **1972**, *39*, 163.
(65) Trasatti, S. *Adv. Electrochem. Electrochem. Eng.* **1977**, *10*, 213.

JP1048887